Finite Element Parametric Study of Reinforced Concrete Beams Shear-Strengthened with Embedded FRP Bars

Michael Qapo

PhD Candidate

mkq118@bham.ac.uk

School of Engineering, University of Birmingham

Edgbaston, Birmingham, B15 2TT, United Kingdom

Samir Dirar (Corresponding author)

Lecturer in Structural Engineering

s.m.o.h.dirar@bham.ac.uk

School of Engineering, University of Birmingham

Edgbaston, Birmingham, B15 2TT, United Kingdom

Yaser Jemaa

Structural Engineer

y.jemaa@outlook.com

Shire Structures, Bromsgrove, B61 0SZ, United Kingdom

Abstract

The deep embedment (DE) of fibre-reinforced polymer (FRP) bars is a promising shear-strengthening scheme for existing concrete structures. In the current study, a three-dimensional nonlinear finite element (FE) model for DE-strengthened reinforced concrete beams was developed and validated. The FE and Concrete Society TR55 predictions were compared with published experimental results. The FE-predicted/experimental shear strength enhancement ratio is 1.08 with a standard deviation of 0.25 whereas the TR55-predicted/experimental shear strength enhancement ratio is 1.57 with a standard deviation of 0.54. A numerical parametric study was carried out. The results showed that the predicted shear strength enhancement was positively influenced by the use of inclined DE FRP bars and the increase in concrete compressive strength but decreased with the increase in shear span-to-effective depth ratio and internal steel stirrup-to-DE FRP bar ratio. The predicted percentage of shear strength enhancement was not significantly influenced by size effect.

1 Introduction

The introduction of fibre reinforced polymer (FRP) reinforcement into the civil engineering industry can be traced back to the 1980s [1-3]. Since then, FRP shear strengthening of concrete structural elements, mainly in the form of externally bonded (EB) sheets or near surface mounted (NSM) bars, has grown dramatically [1-2,4]. However, the shear strength enhancement that can be provided by these systems is negatively affected by premature debonding at a stress level of 20 to 30% of the FRP tensile strength [5-7], especially in the cases of beams with (T) or (I) cross-sections [3]. Hence, unless proper anchorage is provided, it is not usually possible to fully utilise the high tensile strength of the FRP composites [2].

Valerio and Ibell [8] developed the deep embedment (DE) technique, also called the embedded through-section (ETS) method [4,9-11], which overcomes the shortcomings of the

EB and NSM strengthening techniques. In this method, vertical or inclined holes are drilled from the soffit of existing reinforced concrete (RC) structures in the desired shear span. High viscosity epoxy resin is then injected into the drilled holes and FRP or steel bars are inserted into the epoxy-injected holes. The use of FRP bars is favoured as it eliminates the possibility of corrosion of the shear strengthening system [12]. Compared to the EB and NSM techniques, embedding the FRP bars into the concrete core provides higher strengthening effectiveness because the DE method relies on the concrete core to transfer stresses between the concrete and FRP bars. The concrete core provides better confinement and consequently better bond characteristics to overcome the debonding failure usually associated with the other FRP strengthening methods. Other advantages of the DE method over the EB and NSM strengthening methods include higher protection against fire and vandalism; access to the top slab and time-consuming surface preparation are not required and less epoxy consumption [9].

Limited studies have been carried out on the use of DE FRP bars for concrete shear strengthening. Valerio and Ibell [8] studied the effect of diameter, spacing and orientation of DE aramid FRP (AFRP) bars. Their findings confirmed the validity of the DE technique as three of the strengthened beams failed in flexure. Mofidi et al. [9] investigated the effect of presence of steel stirrups as well as surface coating, spacing and diameter of DE carbon FRP (CFRP) bars on the shear strength enhancement. The results showed that plain CFRP bars provided higher strength enhancement than sand-coated CFRP bars. The shear force gain due to the DE CFRP bars increased with the increase in CFRR bar diameter but decreased with the presence of stirrups and the increase in CFRP bar spacing. Qin et al. [11] examined the effectiveness of CFRP bars as DE shear reinforcement for RC T-girders with uncorroded or corroded steel stirrups. The strengthened girders had higher shear strengths than the corresponding unstrengthened ones. However, the efficacy of the strengthening system decreased with increasing the level of stirrup corrosion.

The above review shows that some of the parameters influencing the behaviour of RC beams shear-strengthened with the DE technique, e.g. concrete strength, shear span-to-effective depth (a/d) ratio and effective beam depth, have not been studied. This may be partially attributable to the relatively high cost associated with carrying out physical tests. The use of a carefully developed finite element (FE) model can provide a viable solution to carry out an extensive parametric study on DE FRP shear-strengthened RC girders. In this study, a three-dimensional nonlinear FE model, capable of predicting the overall behaviour of shear-strengthened RC girders with DE FRP bars, is presented. The predictions of the FE model were verified against experimentally tested RC beams [8-9,11]. The FE model was then used to examine numerically the influence of FRP bar orientation, concrete compressive strength, a/d ratio, effective beam depth and interaction between the DE FRP bars and steel stirrups on the predicted shear strength. Furthermore, this paper evaluates the accuracy of the Concrete Society TR55 [13] design guidance.

2 Research significance

The lifetime extension of existing concrete infrastructure is an application of considerable economic importance. It has been estimated that the cost of replacing structurally deficient bridges in Europe, a significant amount of which are RC bridges, is about €400 billion [14]. In the United States, one in nine of the 607,380 bridges have been rated as structurally deficient and $20.5 billion would need to be invested annually to eliminate the bridge deficient backlog by 2028 [15]. This study provides valuable insight into the performance of the DE method, a promising technique for concrete shear-strengthening. In addition to establishing the influence of the main parameters governing the strengthened behaviour; this study identifies limitations in current shear strengthening design guidelines and presents an accurate FE model for predicting both the strength and behaviour of DE shear-strengthened RC structures.

3 Finite element model

A three-dimensional nonlinear FE model was developed using DIANA [16]. Several constitutive models (from the published literature) and element types were tested. Based on the obtained results, the most appropriate ones were selected to develop the FE model. The modelling procedures used in this research are briefly illustrated in the following subsections. For further details about the material models and element types, please see the FE package user's manual [16].

3.1 Geometric modelling

3.1.1 Concrete and steel plates

Three-dimensional eight-node isoparametric solid brick elements [16] were employed for the concrete (see Fig. 1), whereas the loading and support steel plates were represented using three-dimensional six-node isoparametric solid wedge elements [16]. Each node of these elements has three translational degrees of freedom. Several mesh densities were investigated for the concrete and the average mesh size of 30 mm ($3d_a$, where d_a represents the maximum aggregate size of the concrete mix) in each direction was selected. This mesh size, i.e. $3d_a$, has also been recommended by Bažant and Oh [17]. Furthermore, the selected mesh size maintains a balance between accuracy and computational time.

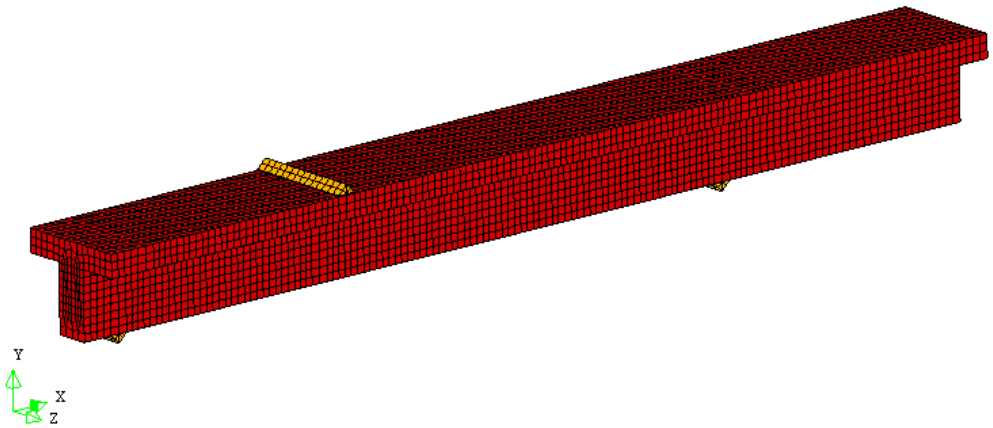

Fig. 1. Finite element model

3.1.2 Steel reinforcement (longitudinal bars and stirrups)

Embedded bar (truss-like) elements [16] were employed to represent the longitudinal reinforcement and shear stirrups. This reinforcement element does not have independent degrees of freedom, and its strains are computed from the displacement field of the concrete elements surrounding it. Recent studies [18,19] demonstrated that, when the failure mode is not controlled by the bond between the steel reinforcement and the concrete, the behaviour of FRP-strengthened concrete structures could be successfully predicted using the perfect bond assumption. In this study, perfect bond was assumed between the internal steel reinforcement and the surrounding concrete as bond failure had not been observed during the experimental tests [8,9,11], which are presented in Section 4.1.

3.1.3 FRP bars

The FRP bars were represented using three-dimensional two-node truss elements [16]. These elements are only deformable in the axial direction, whilst bending and shear deformations are not allowed.

3.1.4 FRP bar-to-concrete interface

For modelling the bond area (i.e. interface region) between the FRP bars and the surrounding concrete, four-node three-dimensional interface elements [16] were employed. These elements linked the edges of the solid elements, which represented the concrete, to the truss elements which were used to model the DE FRP bars. The four-node three-dimensional interface elements permitted the relative displacements, i.e. the slip, between the concrete and the DE FRP bars to be modelled.

3.2 Material modelling

3.2.1 Concrete

A total strain rotating crack model (a smeared crack based model) was employed for simulating the concrete. In the adopted rotating crack model, the concrete behaviour in

tension and compression is described with one stress-strain curve [16]. The stress-strain curve of Thorenfeldt et al. [20] was used in compression, which is given by:

$$\frac{f_c}{f_c'} = \frac{n\left(\frac{\varepsilon_c}{\varepsilon_{co}}\right)}{n - \left(1 - \left(\frac{\varepsilon_c}{\varepsilon_{co}}\right)^{nk}\right)} \qquad (1)$$

where f_c represents the concrete compressive stress at a specific strain ε_c, f_c' is the concrete cylinder compressive strength, ε_{co} (automatically determined by DIANA) is the strain at f_c', n is a parameter equal to $0.18 + (f_c'/17)$ and k is a parameter governing the descending branch of Equation 1 and is equal to $0.67 + (f_c'/62)$). The softening of concrete in compression, as a result of lateral cracking, was incorporated by adopting the model developed by Vecchio and Collins [21].

The concrete tensile behaviour was modelled using a linear relationship up to concrete cracking. A linear tension softening model (based on fracture energy, G_f) was used to simulate the gradual drop in tensile stress after concrete cracking. The fracture energy was calculated using Remmel's model [22]:

$$G_f = 0.065 \times \ln\left(1 + \frac{f_c'}{10}\right) \qquad (2)$$

An explicit model to simulate the shear behaviour of concrete after cracking was not required because, in the rotating crack model, the direction of the crack changes according to the change in the principal tensile stress direction. It follows that any crack plane in this model is a principal plane and consequently there are no shear stresses acting on this plane. Poisson's ratio of concrete was taken as 0.15, which is consistent with the recommendations of CEB-FIP Model Code 1990 [23].

3.2.2 Steel reinforcement, steel plates and FRP bars

An elastic-perfectly plastic stress-strain model was adopted for the internal steel reinforcement, as well as the steel plates (i.e. loading and support plates). For the FRP bars,

a linear-brittle stress-strain model, based on the ultimate strength values reported in the experimental tests [8,9,11], was used.

3.2.3 FRP bar-to-concrete interface

The two-part bond-slip model of Mofidi et al. [9] was adopted to represent the behaviour of the interface behaviour between the FRP bars and concrete. The bond-slip model is used to represent the overall FRP bar-to-concrete interface behaviour rather than that of the adhesive material. The ascending branch of this model is defined by a parabolic bond stress-slip relationship, up to the bond strength (τ_m), and given by:

$$\tau = \tau_m \left(\frac{s}{s_m}\right)^{\alpha} \qquad (3)$$

The descending branch is described by the following linear relationship:

$$\tau = \tau_m \left(1 + p - p\frac{s}{s_m}\right) \qquad (4)$$

where τ is the bond stress at a specific slip s, s_m is the slip value at τ_m, α is a curve-fitting parameter and p is a parameter controlling the descending part of the bond-slip relationship. For sand-coated CFRP bars, τ_m, s_m, α and p may be taken as 8.4 MPa, 0.08 mm, 0.09 and 0.07, respectively [9].

It should be noted that the beams tested by Valerio and Ibell [8] were strengthened with DE AFRP bars (see Section 1). Due to the lack of a bespoke bond stress-slip model for the DE AFRP bars, the above bond stress-slip model was adopted for these beams as perfect bond between the AFRP bars and the concrete was deemed inappropriate. It is believed that the use of the above bond-slip model had insignificant implications on the modelled behaviour as none of the beams tested by Valerio and Ibell [8] failed due to debonding of the AFRP bars.

3.3 Solution algorithm

An appropriate incremental-iterative procedure was adopted to solve the nonlinear equations. The vertical loads were applied as displacement increments and, for each increment, the Quasi-Newton iterative method (also known as the Secant method) was employed alongside a displacement-based convergence criterion. The displacement norm value of 0.1% was chosen based on the work of Hee and Jefferson [24]. Convergence was successfully achieved at the end of each load step using this procedure. A similar solution algorithm was successfully used by Qapo et al. [19].

4 Model validation

Three sets of experimentally tested RC beams were used for model validation. All considered beams failed in shear. Table 1 shows the material properties of the RC beams.

Table 1. Material properties of the tested RC beams

RC beam set	Material	Elastic modulus (MPa)	Cylinder compressive strength (MPa)	Ultimate strain mm/mm	Yield strength (MPa)	Ultimate strength (MPa)
Set 1 – includes: S0-CON, S0-12d130s, S1-CON and S1-12d260s [9]	Concrete	-	25[1]	-	-	-
	Ø8 mm stirrups	200,000	-	-	540	-
	Ø10 mm bars	200,000	-	-	470	-
	Ø25 mm bars	200,000	-	-	470	-
	Sand-coated CFRP	148,000	-	0.0127	-	1885
Set 2 – includes: N00 and R00 [11]	Concrete (N00)	-	21	-	-	-
	Concrete (R00)	-	17.4	-	-	-
	Ø8 mm (test span)	186,000	-	-	542	-
	Ø8 mm (other)	183,000	-	-	573	-
	Ø20 mm bars	179,000	-	-	576	-
	Ø25 mm bars	180,000	-	-	537	-
	Sand-coated CFRP	124,000	-	0.0175	-	2172
Set 3 – includes: Specimens 1, 8, 9 and 10 [8]	Concrete	-	47[2]	-	-	-
	Ø12 mm bars	200,000	-	-	635	-
	Sand-coated AFRP	60,000	-	0.0240	-	1440

[1] The cylinder compressive strength of S1-12d260s was 29.6 MPa.
[2] The cylinder compressive strength of Specimen 1 was 41 MPa.

4.1 Details of test specimens

The first set comprised the four RC T-beams S0-CON, S1-CON, S0-12d130s and S1-12d260s [9]. S0-CON and S1-CON were unstrengthened control beams whereas S0-12d130s and S1-12d260s were strengthened in shear using DE CFRP bars. The beams, which had a/d ratio of 3.0, were 4520 mm long and tested in three-point-bending as illustrated in Fig. 2. The beams had overall depth, flange width, web width and flange thickness of 406 mm, 508 mm, 152 mm and 102 mm respectively. Each beam was reinforced in tension with four Ø25 mm steel bars, whilst six Ø10 mm steel bars were used as compression reinforcement (see Fig. 3). S0-CON had no internal steel shear reinforcement, while S1-CON had Ø8 mm steel shear links spaced at 175 mm centre-to-centre (c/c). S0-12d130s had no shear links and was strengthened in shear using Ø12.7 mm DE CFRP bars spaced at 130 mm c/c. S1-12d260s had Ø8mm internal steel shear links spaced at 175 mm c/c and Ø12.7 mm DE CFRP bars spaced at 260 mm c/c.

The second set included the two RC T-beams N00 and R00 [11]. The beams were 2700 mm long (with a total span of 2200 mm) and were tested in three-point-bending with a/d ratio of 3.05. The web width, flange width and flange thickness were 125 mm, 260 mm and 100 mm, respectively. The beams had an effective depth of 295 mm. The longitudinal bars comprised three Ø20 mm in compression and four Ø25 mm in tension. Both beams had Ø8 mm steel shear links spaced at 275 mm c/c in the deficient shear span and 100 mm c/c elsewhere. N00 was an unstrengthened control beam whereas R00 was strengthened with Ø10 mm sand-coated CFRP bars with a centre to centre spacing of 275 mm.

The third set included Specimens 1, 8, 9 and 10 tested by Valerio and Ibell [8]. Specimen 1 was an unstrengthened control beam. Specimens 8, 9 and 10 had two Ø10 mm, two Ø7.5 mm and one Ø10 mm sand-coated AFRP bars in each shear span respectively. The beams, which had a/d ratio of 3.17, were 3000 mm long (with a total span of 2250 mm) and were tested in a four-point-bending configuration. They had a rectangular cross-section with a width, effective depth and total depth of 110 mm, 189 mm and 220 mm respectively. In this

series, each beam was reinforced in tension with two Ø12 mm high yield steel bars. The beams had no steel compression or shear reinforcement.

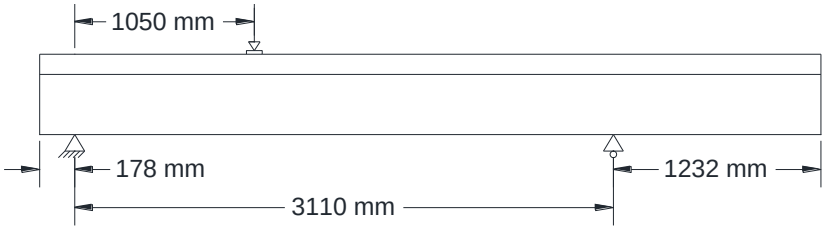

Fig. 2. Details of the tested RC T-beams [9]

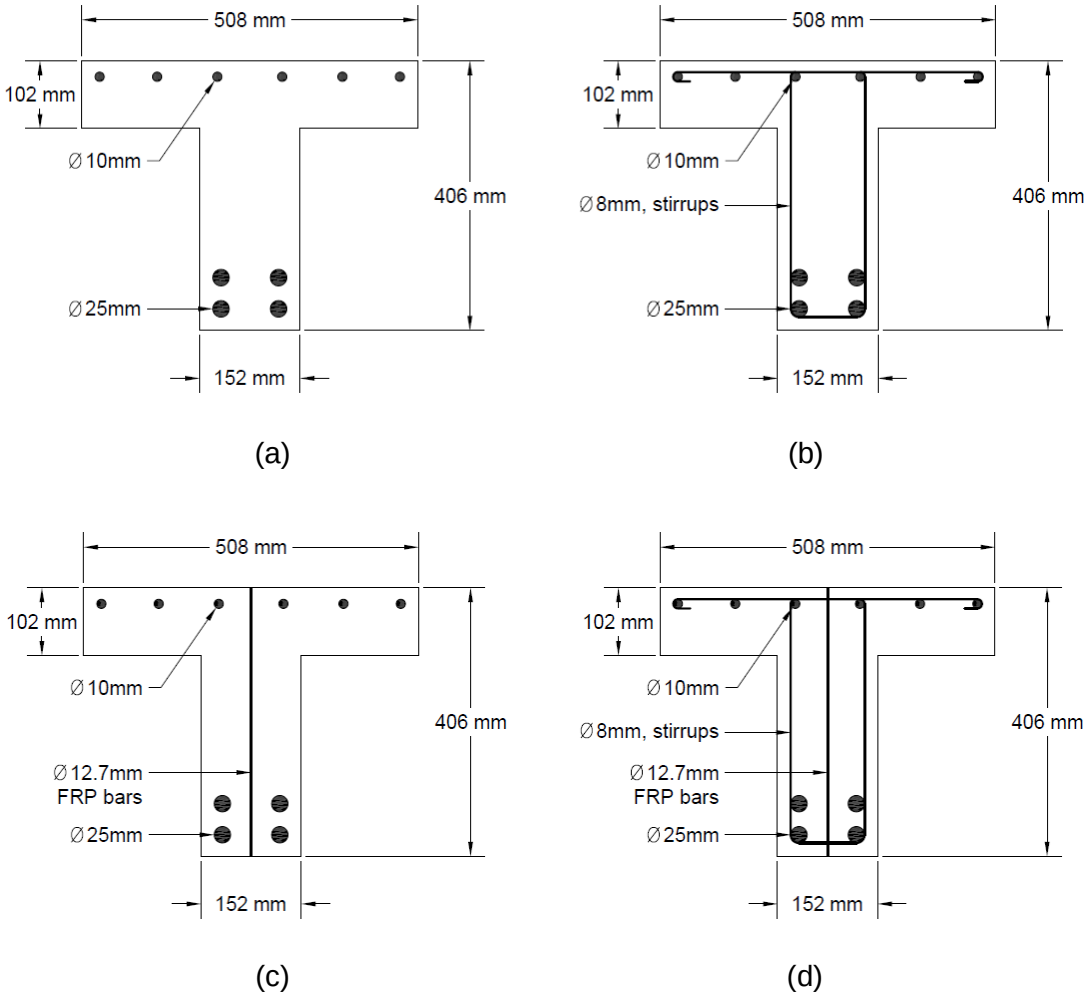

Fig. 3. Cross-section dimensions of the tested T-beams: (a) S0-CON, (b) S1-CON, (c) S0-12d130s and (d) S1-12d260s [9]

4.2 Finite element model predictions

The accuracy of the FE model was evaluated by comparing the experimental results with the FE predictions. The comparison included the shear force capacity, deflection response, strain in stirrups and FRP bars and crack patterns at failure.

The experimental and FE-predicted shear strengths are given in Table 2. The overall mean predicted/experimental shear force capacity ratio and standard deviation are respectively 1.02 and 0.05. The best predictions were obtained for the first set of beams [9] which had a mean predicted/experimental shear force capacity ratio of 1.00 and a standard deviation of 0.02. Only the first set included RC beams with different shear links ratios (0 and 0.38%). Furthermore, the first set included beams with a T cross-section which adequately simulates the common slab-on-beam construction method. Thus, the first set of beams form the basis of the parametric study reported in Section 6.

Table 2. Experimental and FE-predicted shear force capacities

Beam	Shear force capacity, V (kN)		FE/Exp. [1]
	Experimental	FE analysis	
S0-CON [9]	81.3	80.5	0.99
S0-12d130s [9]	180.8	176.9	0.98
S1-CON [9]	232.2	234.5	1.01
S1-12d260s [9]	266.6	271.5	1.02
N00 [11]	143.0	133.4	0.93
R00 [11]	142.0	150.6	1.06
Specimen 1 [8]	22.5	25.4	1.13
Specimen 8 [8]	32.0	33.3	1.04
Specimen 9 [8]	32.0	31.9	1.00
Specimen 10 [8]	30.0	31.5	1.05

[1] Mean (FE/Exp.) value is 1.02 with a standard deviation of 0.05.

The experimental and numerical variations of shear force with deflection under loading point for the beams tested by Mofidi et al. [9] are depicted in Fig. 4. The Figure shows that all curves are approximately linear up to crack formation. Subsequently, the curves turned nonlinear as a result of stiffness deterioration due to cracking. The deterioration continued

with increased loading until failure occurred. At failure, the load dropped suddenly which is a characteristic of shear failure. Fig. 4 clearly demonstrates that there is a very good match between the experimental and FE-predicted shear force-deflection behaviour from initial loading up to beam failure. This result further confirms the accuracy of the FE model.

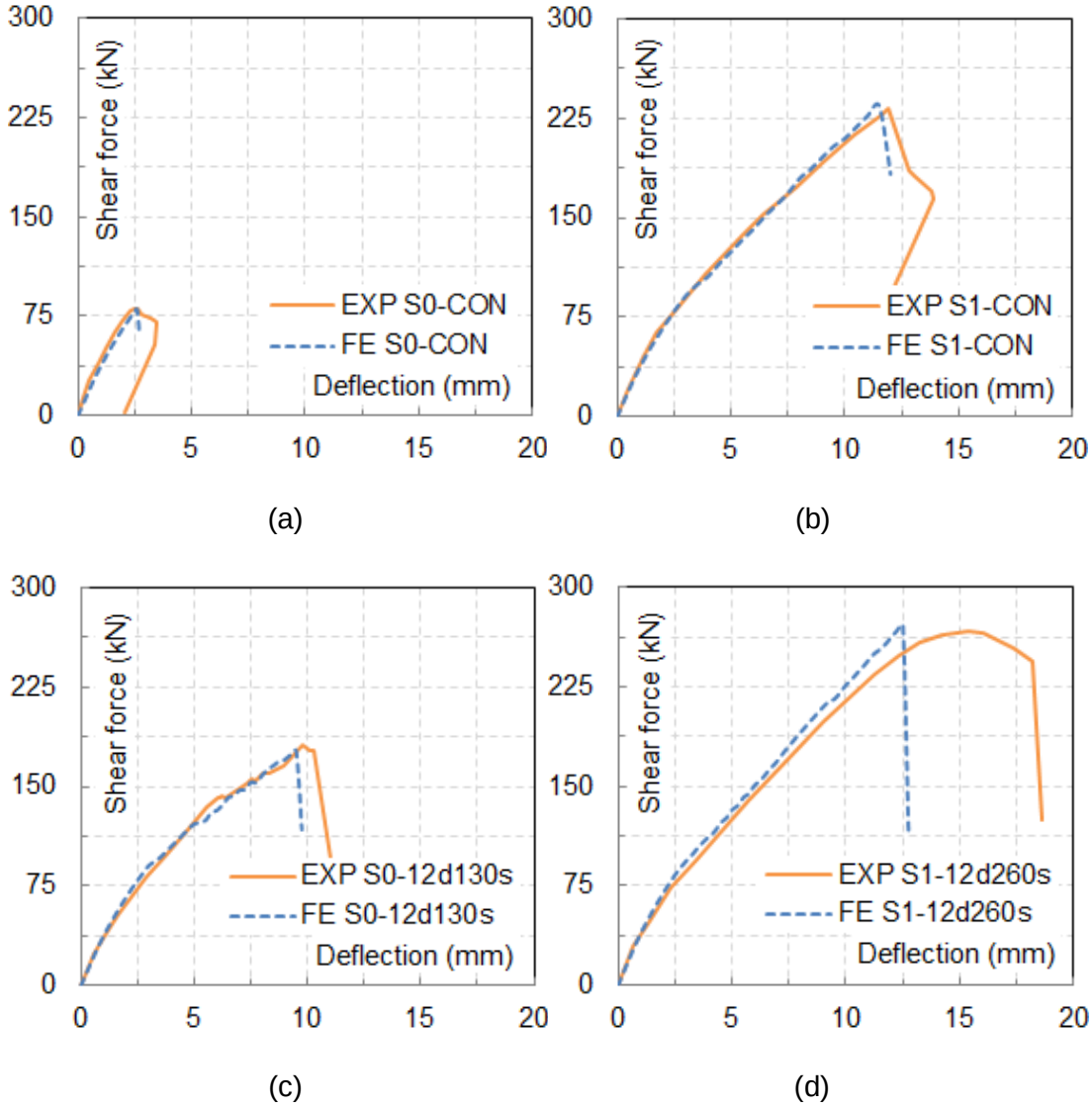

Fig. 4. Experimental [9] and FE-predicted shear force-deflection curves: (a) S0-CON, (b) S1-CON, (c) S0-12d130s and (d) S1-12d260s

The variations of shear force versus maximum strain in the steel stirrups and DE CFRP bars are presented in Fig. 5 and Fig. 6, respectively. The developed FE model correctly predicted that both the shear stirrups and DE CFRP bars remained passive up to the formation of inclined cracks. The developed model also correctly predicted the shear forces (50-75 kN) at

which the steel and CFRP shear reinforcement started to develop strain. The development of strain in the steel shear links was overall well modelled, whilst the strain in the DE CFRP bars was underestimated. This may be attributable to the smeared modelling of the discrete shear cracks. Nonetheless, the FE model successfully captured the main characteristics of the experimental behaviour which included yielding of the steel shear links, absence of DE CFRP bar debonding and brittle (shear) failure.

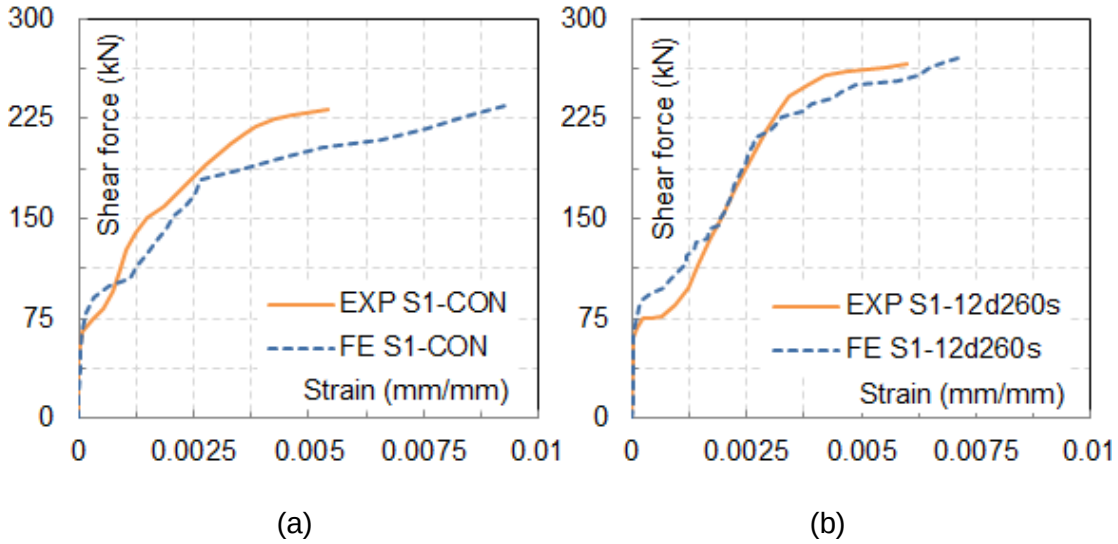

(a) (b)

Fig. 5. Experimental [9] and FE-predicted shear force vs. strain in the steel shear links: (a) S1-CON and (b) S1-12d260s

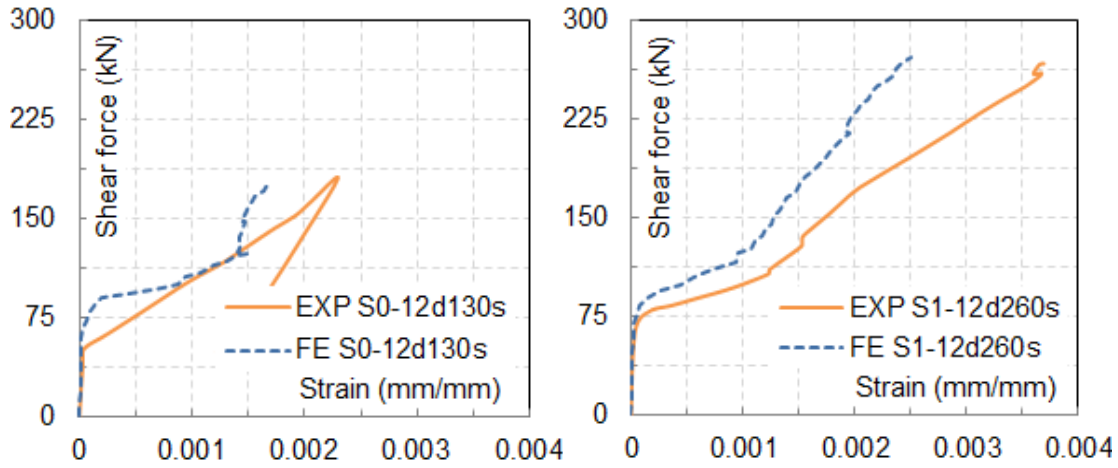

(a) (b)

Fig. 6. Experimental [9] and FE-predicted shear force vs. strain in the DE CFRP bars: (a) S0-12d130s and (b) S1-12d260s

Mofidi et al. [9] did not provide figures for the experimental crack patterns at failure of the modelled beams. However, they reported that failure of S1-12d260s occurred when parallel diagonal shear cracks, that formed at relatively equal distances with an inclination angle of 37°-42°, opened up and reached the flange of the beam. This description is quite comparable to the predicted principal tensile strain contours at failure of S1-12d260s, which are shown in Fig. 7.

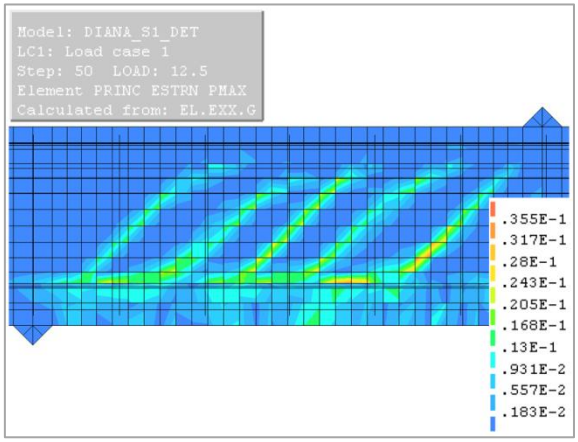

Fig. 7. Predicted principal tensile strain contours for S1-12d260s at failure

For the beams tested by Qin et al. [11], the experimental and FE-predicted shear force versus deflection under loading point curves are shown in Fig. 8. The stiffer behaviour predicted for R00 can be attributed to the FRP-to-concrete bond-slip model [25-26].

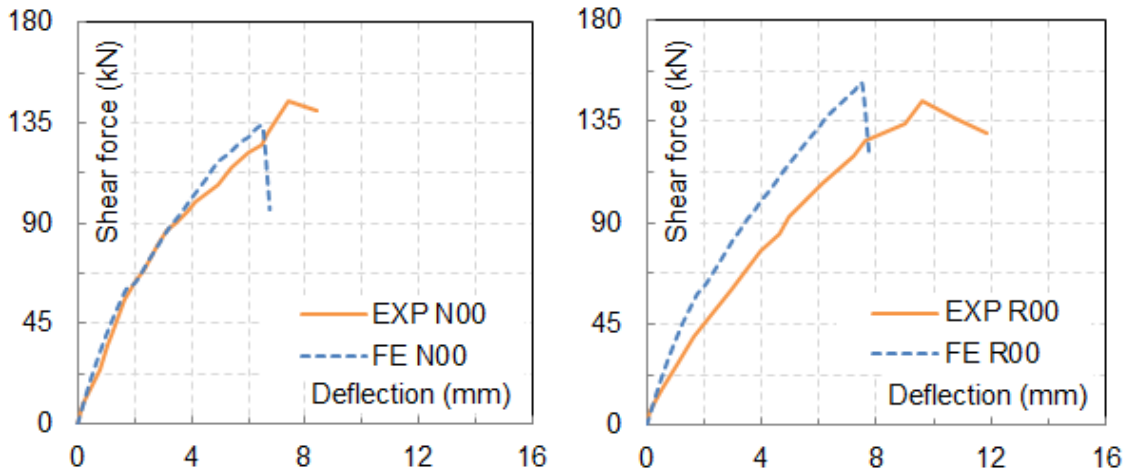

Fig. 8. Experimental [11] and predicted shear force-deflection curves: (a) N00 and (b) R00

The experimentally tested beams failed in shear. There was no sign of FRP debonding for R00. This behaviour was accurately predicted by the developed FE model as can be seen in Fig. 9 which compares the experimental and FE-predicted failure modes for R00. Fig. 10 shows that the FE model correctly predicted the shear force-strain variation for the middle steel stirrup in R00. The strain results for the DE FRP bars in R00 were not published.

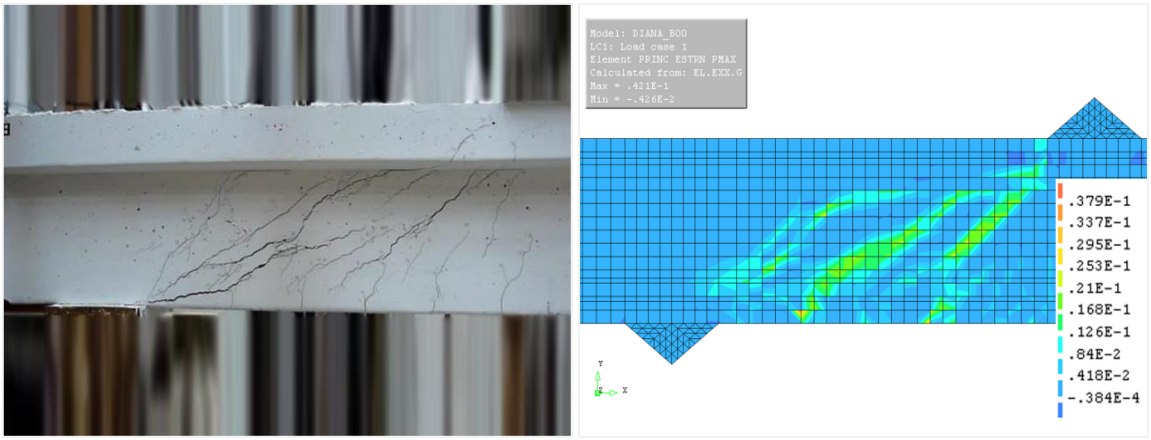

Fig. 9. Experimental [11] and FE-predicted failure modes of R00

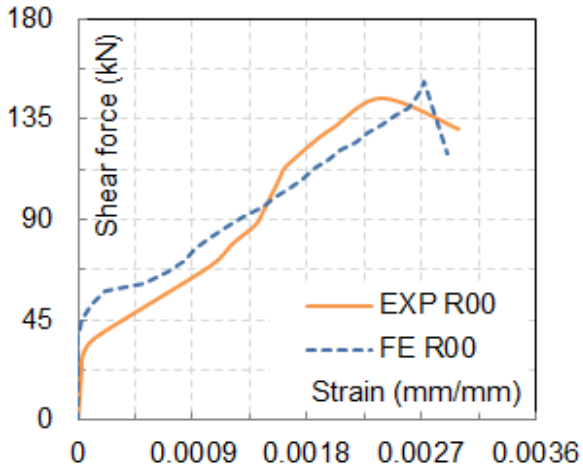

Fig. 10. Experimental [11] and FE-predicted shear force-strain variation for the middle steel stirrup in R00

Fig. 11 compares the experimental and FE-predicted shear force versus mid-span deflection curves for the beams tested by Valerio and Ibell [8]. The available experimental and the corresponding FE-predicted failure modes are compared in Fig. 12. Based on the presented

comparisons, it can be concluded that the developed FE model successfully captured the experimental behaviour of both the control and the strengthened beams with high accuracy.

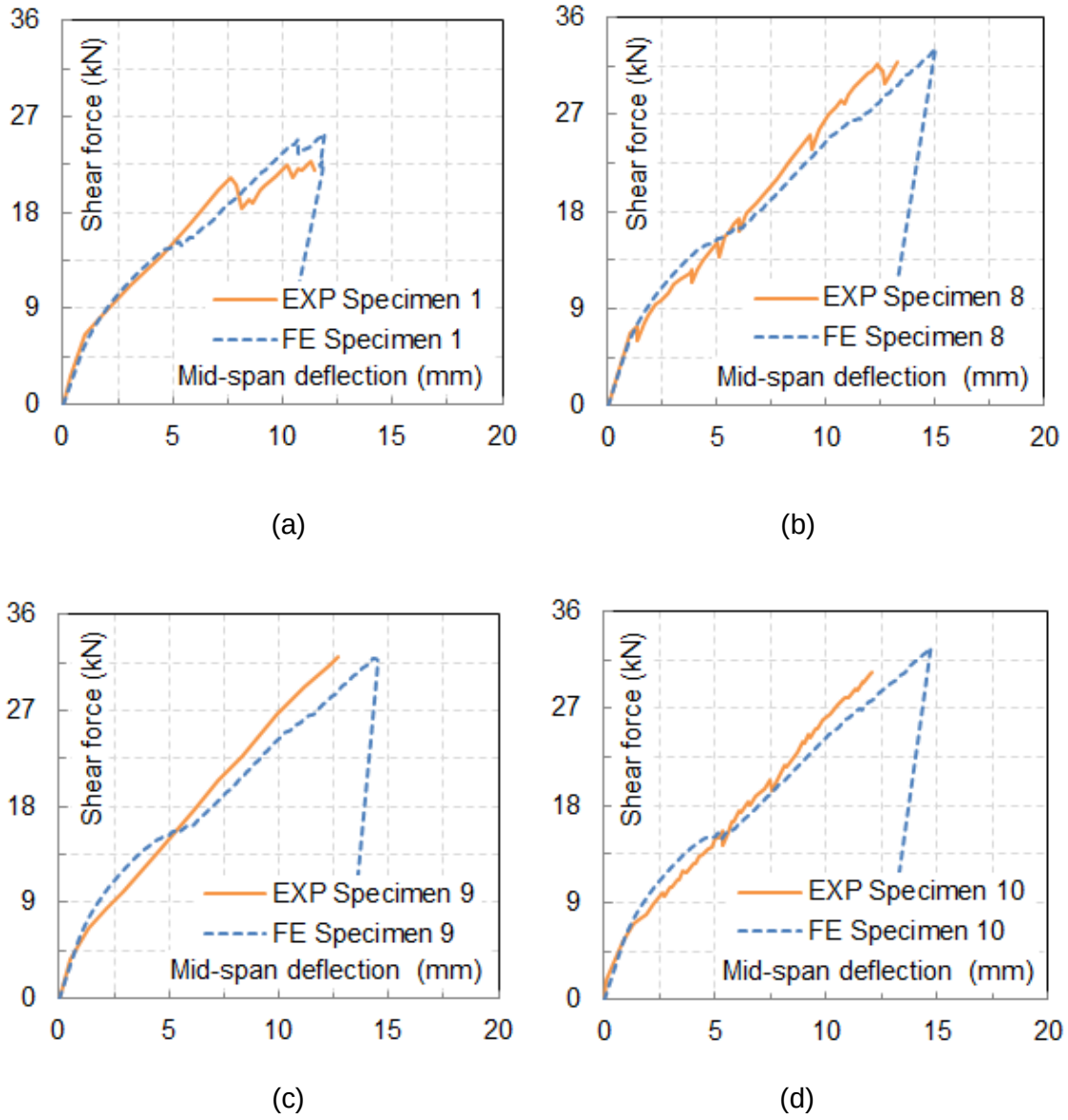

Fig. 11. Experimental [8] and FE-predicted shear force-deflection curves: (a) Specimen 1, (b) Specimen 8, (c) Specimen 9 and (d) Specimen 10

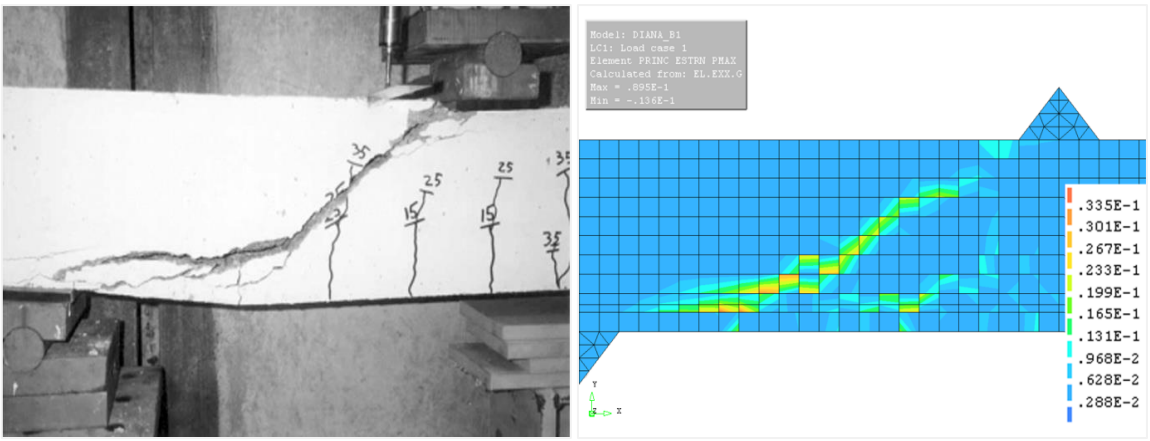

(a)

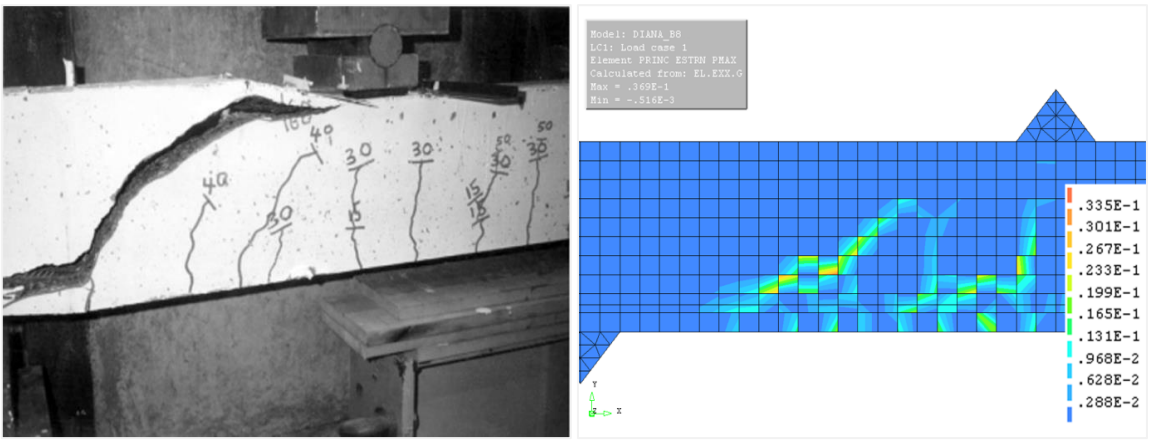

(b)

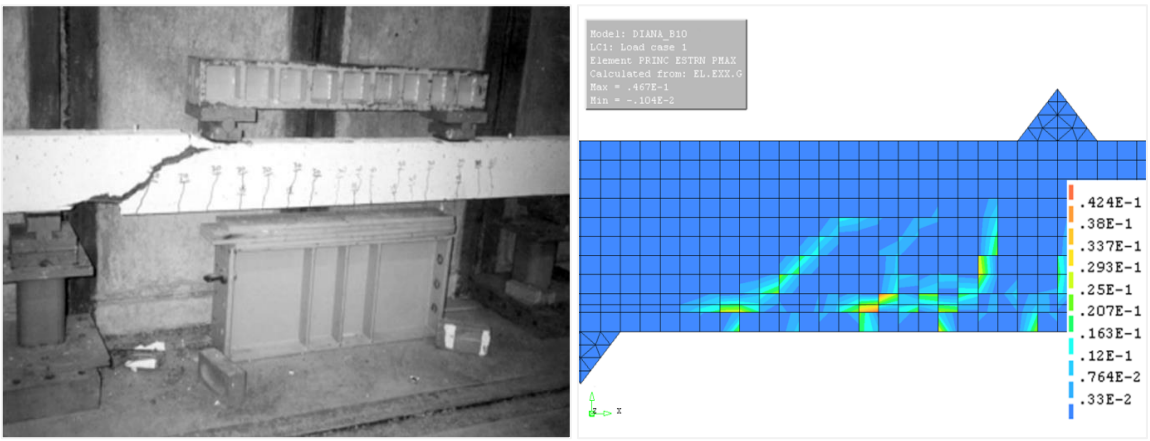

(c)

Fig. 12. Experimental [8] and FE-predicted failure modes: (a) Specimen 1, (b) Specimen 8 and (c) Specimen 10

5 Comparison of experimental results with FE and TR55 predictions

The Concrete Society's [13] Technical Report 55 (TR55) is the first, and currently the sole, standard document to provide detailed design guidelines for DE FRP shear reinforcement. TR55 suggests the following expression for the shear force carried by DE FRP bars (V_f):

$$V_f = \frac{\varepsilon_{fse} E_{fd} A_f}{s_b} W_{eff} \qquad (5)$$

where ε_{fse} is the effective strain in the FRP bars (taken as 0.004 mm/mm), E_{fd} is the design Young's modulus of the FRP bars (MPa), A_f represents the area of one FRP bar (mm^2), s_b represents the spacing between the FRP bars (mm) and W_{eff} is the effective width (mm) over which the FRP bars may act and given by:

$$W_{eff} = h - 2l_{b,max} \qquad (6)$$

where h is the strengthened depth (mm) and $l_{\mathrm{b,max}}$ is the maximum anchorage length (mm) beyond which no additional capacity gain can be achieved, given by:

$$l_{b,max} = \frac{\varepsilon_{fse} E_{fd} A_f}{\left(\pi d_b \frac{\tau_b}{\gamma_A}\right)} \qquad (7)$$

where d_{b} is the FRP bar diameter (mm), τ_{b} represents the average bond stress (MPa) over the anchored length and can be taken as 15 MPa in the absence of test data and γ_{A} is a partial safety factor for the adhesive material.

A comparison of the experimental results with FE and TR55 predictions for V_f is presented in this section. All safety factors are set equal to 1.00 for the purpose of comparison. The experimental and numerical (FE) values of V_f were calculated by subtracting the shear strength of an unstrengthened beam from the shear strength of the corresponding strengthened beam. Differences in the concrete strength between the control and strengthened beams (see Table 1) were taken into consideration when calculating the experimental and numerical (FE) values of V_f.

Table 3 compares the shear force gain predicted by the FE model and TR55 design model with the experimental results. TR55 predictions overestimated the shear force gain with a mean predicted/experimental ratio of 1.57 and a standard deviation of 0.54. The discrepancy of TR55 predictions may be attributable to the relatively high value of average bond stress (15 MPa) allowed by the design guidance. Thus, the TR55 model underestimates the value of the anchorage length ($l_{\mathrm{b,max}}$) and consequently overestimates both W_{eff} and V_f. The FE model gave much better predictions for the shear force gain with a mean predicted/experimental ratio of 1.08 and a standard deviation of 0.25.

Given the importance of TR55 [13] as the only standard document that provides detailed design guidance for DE FRP shear reinforcement, improving the accuracy of its predictions is urgently needed.

Table 3. Experimental, FE and TR55 shear force gain

Beam	Shear force gain due to FRP bars (kN)			$V_{f,FE}$ / $V_{f,exp}$ [2]	$V_{f,TR55}$ / $V_{f,exp}$ [3]
	Experimental $V_{f,exp}$ [1]	FE model $V_{f,FE}$ [1]	TR55 [13] $V_{f,TR55}$		
S0-12d130s [9]	99.5	96.4	89.4	0.97	0.90
S1-12d260s [9]	20.3	28.0	44.7	1.38	2.20
R00 [11]	11.8	17.0	27.5	1.44	2.33
Specimen 8 [8]	8.4	7.9	13.2	0.94	1.57
Specimen 9 [8]	8.4	6.5	8.5	0.77	1.01
Specimen 10 [8]	6.4	6.1	8.8	0.95	1.38

[1] Calculated taking into consideration differences in concrete strength between the control and strengthened beams (see Table 1).
[2] Mean ($V_{f,FE}$ / $V_{f,exp}$) value is 1.08 with a standard deviation of 0.25.
[3] Mean ($V_{f,TR55}$ / $V_{f,exp}$) value is 1.57 with a standard deviation of 0.54.

6 Parametric study

Based on the demonstrated accuracy of the developed FE model, a numerical parametric study was executed to study the effect of DE FRP bar inclination angle, concrete compressive strength, a/d ratio, effective beam depth and interaction between steel stirrups and DE FRP bars on the predicted shear strength. As explained in Section 4.2, the

parametric study was based on beams tested by Mofidi et al. [9]. Where appropriate, FE and TR55 [13] predictions are compared and similarities and differences are highlighted.

Of note is that the FE predictions reflect the performance of the developed model. Further experimental tests are required to confirm the FE predictions.

6.1 DE FRP bar orientation

The effect of DE FRP bar orientation was investigated by modelling beams nominally identical to S0-12d130s and S1-12d260s. For each modelled beam, the DE FRP bars were inclined at either 45° or 90° to the longitudinal beam axis.

Table 4 presents the FE-predicted results. The predicted shear force capacities of the beams without (S0-12d130s) and with (S1-12d260s) internal steel stirrups increased by 12.5% and 4.3%, respectively when the DE FRP bar inclination angle was changed from 90° to 45°. This outcome is in broad agreement with the work of Barros and Dalfré [10] who reported that inclined DE steel bars were more efficient compared with vertical ones, especially for the case of RC beams without internal steel stirrups. The higher strength enhancement offered by inclined DE bars may be attributable to two reasons. First, inclined DE bars are less susceptible to debonding owing to the higher anchorage length. Second, for the same values of A_f, b_w (web width) and s_b; the shear reinforcement ratio of inclined DE bars ($A_f/b_w S_b Sin\theta$), where θ is the DE bar inclination angle, is higher than that of vertical bars ($A_f/b_w S_b$). Thus, inclined DE bars offer higher resistance to crack opening than vertical DE bars.

Table 4. Effect of DE FRP bar orientation

Beam	Shear force capacity, V (kN)		Increase attained by inclined bars (%)
	Vertical DE bars (90°)	Inclined DE bars (45°)	
S0-12d130s	176.9	199.0	12.5
S1-12d260s	271.5	283.1	4.3

TR55 design model [13] does not consider the influence of DE FRP bar orientation on the shear strength enhancement. Therefore, it was not possible to compare the FE results for beams with inclined DE FRP bars with TR55 predictions.

6.2 Concrete cylinder compressive strength

The effect of concrete compressive strength was studied by modelling beams nominally identical to S0-CON, S0-12d130s, S1-CON and S1-12d260s. For each beam, concrete cylinder compressive strength values of 25, 35, 45, 55 and 65 MPa were considered.

Fig. 13a and Fig. 13b present the influence of concrete cylinder compressive strength on the predicted shear force at failure and shear force contribution of the DE FRP bars, respectively. Some of the FE models for S1-CON and S1-12d260s failed in flexure and their predictions were discarded. All the remaining predictions presented in Fig. 13 are for FE models that failed in shear.

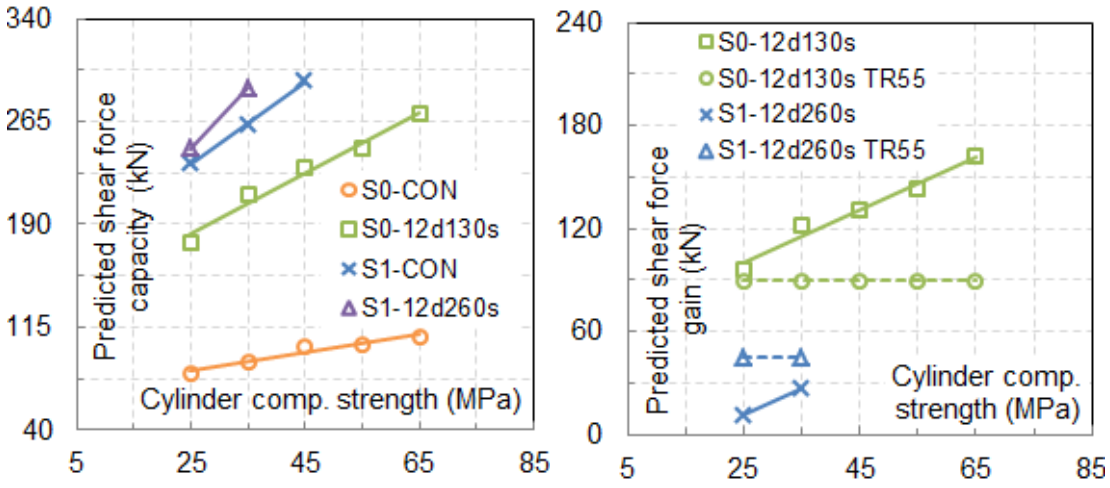

(a) (b)

Fig. 13. Influence of concrete cylinder compressive strength on the predicted (a) shear force capacity and (b) gain in shear force attributable to DE FRP bars

Fig. 13a shows that the predicted shear strength increased linearly with the increase in concrete grade. The predicted shear strength increased respectively by 33.8% and 52.8% for the unstrengthened (S0-CON) and strengthened beams without steel shear

reinforcement (S0-12d130s) when the concrete compressive strength was increased from 25 to 65 MPa. For the unstrengthened beam with steel shear reinforcement (S1-CON), increasing the concrete cylinder compressive strength from 25 to 45 MPa resulted in an increase in the predicted shear force capacity by 26.1%. The predicted shear force capacity increased by 18.3% for the strengthened beam with steel shear reinforcement (S1-12d260s) as a result of increasing the concrete cylinder compressive strength from 25 to 35 MPa. The predicted increases in the shear force capacities may be attributable to the enhancement in the concrete shear force contribution as a result of increasing the grade of concrete.

Fig. 13b shows that the higher the concrete grade, the higher the predicted shear strength enhancement due to the DE FRP bars. Due to the good bond between the concrete and DE FRP bars, which is represented by the bond-slip model, bond failure does not occur. The weakest link becomes the concrete next to the FRP-to-concrete interface. Increasing the concrete grade results in a corresponding increase in the concrete tensile strength and this, in return, improves the DE FRP contribution. The predicted shear contribution of the DE FRP bars increased from 96.4 kN to 162.6 kN for the beams without steel stirrups as a result of the increase in concrete grade from 25 to 65 MPa. For the beams with steel stirrups, increasing the concrete grade from 25 to 35 MPa resulted in an increase in the predicted shear force gain from 11.2 kN to 26.8 kN.

As demonstrated in Fig. 13b, TR55 design model [13] does not consider the influence of concrete compressive strength on the shear strength enhancement provided by DE FRP bars.

6.3 Shear span-to-effective depth ratio

The a/d ratio has a substantial effect on the shear behaviour of RC beams as the change in a/d ratio results in a change in the shear resisting system. RC beams with an a/d ratio less than 2.5 (i.e. deep beams) behave as a tied arch after crack formation. The tied arch system

results in direct transfer of the shear force into the support. In contrast, RC beams with a/d ratio higher than 2.5 (i.e. slender beam) resist shear by beam action [27].

Sayed et al. [28] and Qapo et al. [19] recently assessed the influence of a/d ratio on the shear behaviour of reinforced and prestressed concrete girders strengthened by EB CFRP sheets, respectively. The results showed that the shear contribution of the EB CFRP sheets was substantially influenced by the a/d ratio of the beam. The influence of a/d ratio on the shear contribution of DE FRP bars has not been investigated.

The influence of a/d ratio was investigated in this study by developing FE models nominally identical to S0-CON, S0-12d130s, S1-CON and S1-12d260s. For each modelled beam, a/d ratios in the range from 2.6 to 4.1 were considered. FE models with a/d ratios higher than 4.1 failed in flexure and thus their predictions were discarded.

The effect of a/d ratio on the predicted average shear stress in the concrete at beam failure is depicted in Fig. 14a. The Figure shows that increasing the a/d ratio leads to a reduction in the predicted average shear stress at failure, which is compatible with the results reported by Kani et al. [27], Sayed et al. [28] and Qapo et al. [19]. This finding might be attributable to the switch in the shear resisting mechanism from arch-action to beam-action. The maximum reduction was about 28.3% for S1-12d260s series.

Fig. 14b shows that increasing the a/d ratio has a negative impact on the predicted shear force gain due to DE FRP bars. The predicted shear force gain due to DE FRP bars decreased approximately linearly by 36.4% and 64.4%, for S0-12d130s and S1-12d260s series respectively, as a result of increasing the a/d ratio from 2.6 to 4.1. This outcome is compatible with the findings of Sayed et al. [28] who modelled EB FRP shear-strengthened RC beams and Qapo et al. [19] who modelled EB CFRP shear-strengthened prestressed concrete beams.

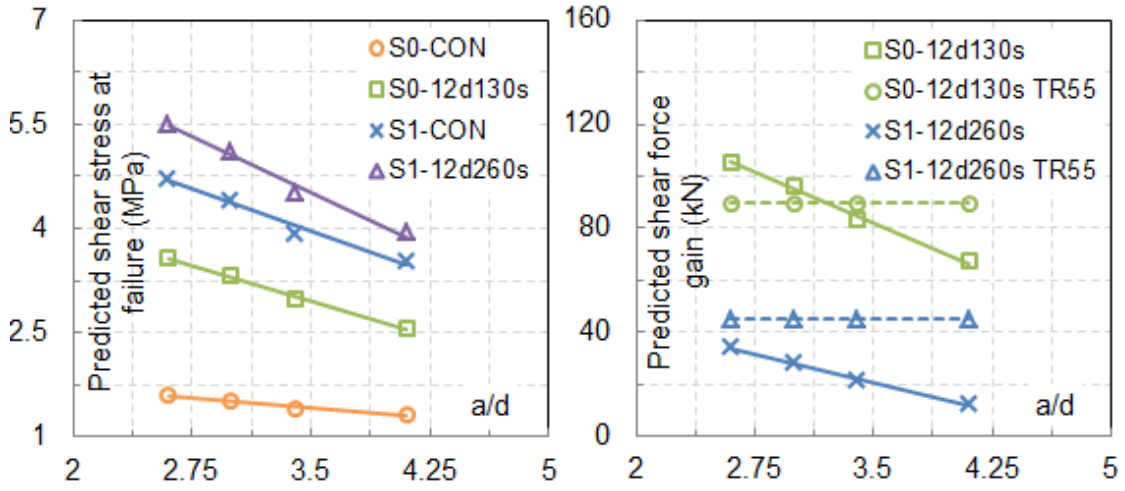

(a) (b)

Fig. 14. Effect of a/d ratio on the predicted (a) shear stress at failure and (b) gain in shear force attributable to DE FRP bars

As shown in Fig. 14b, TR55 design model [13] does not take into account the effect of a/d ratio. This shortcoming needs urgent attention since a/d ratio is one of the key parameters governing the strengthened behaviour.

6.4 Effective beam depth

Previous studies on concrete beams [29,30] have shown that the nominal shear stress at failure tends to decrease with increasing beam depth. This is attributable to wider cracks in larger sections [6]. Moreover, studies on concrete beams shear-strengthened with EB FRP laminates have revealed that the increase in beam depth can have a detrimental influence on the shear contribution of the FRP reinforcement [19,31]. The influence of effective beam depth has not been studied in beams shear-strengthened using DE FRP bars.

In this study, FE models with effective depths of 350 mm (i.e. 1.0d), 525 mm (i.e. 1.5d) and 700 mm (i.e. 2.0d) were developed for S0-CON, S0-12d130s, S1-CON and S1-12d260s in order to study the influence of effective beam depth. The flange dimensions were also changed proportionally with the change in beam depth, whereas other parameters (e.g. a/d

ratio, longitudinal steel ratio, stirrup ratio, DE FRP bar ratio and mesh size) were kept constant.

The influence of effective beam depth on the predicted ultimate shear stress is depicted in Fig. 15a. The Figure shows that the predicted shear stress at failure decreases with increasing effective beam depth. The predicted shear stress at failure decreased respectively by 19.1%, 20.7%, 25.2% and 20.5% for S0-CON, S0-12d130s, S1-CON and S1-12d260s when the effective depth of the beams was doubled. This result is consistent with the findings of previous studies [19,29-31] and may be explained by the wider cracks in larger members.

Fig. 15b presents the effect of effective beam depth on the shear strength enhancement percentage. The percentage of the predicted shear force gain decreased from 119.7% and 12.2% to 115.3% and 9.5% for series S0-12d130s and S1-12d260s, respectively, when the effective depth of the beams was doubled. This result is important because it suggests that beam depth does not significantly affect the shear strength enhancement offered by the DE FRP bars.

Fig. 15c compares the FE-predicted shear strength enhancement results with TR55 [13] predictions. This Figure shows that both the FE and TR55 [13] models predict that the shear strength enhancement increases with increasing beam depth. This may be explained by the increase in effective bond length in large beams [32]. It can also be observed from Fig. 15c that in the case of strengthened beams with steel stirrups (i.e. S1-12d260s series), TR55 model [13] predicted much higher shear strength enhancement levels than the FE model. According to the FE results, the shear force gain increased from 96.4 kN and 28.0 kN to 302.2 kN and 75.3 kN for series S0-12d130s and S1-12d260s, respectively, when the effective depth of the beams was doubled. The corresponding increases predicted by TR55 model [13] were from 89.8 kN and 44.7 kN to 357.7 kN and 178.8 kN, respectively. The values predicted by TR55 [13], especially for S1-12d260s series, seem unrealistically high. As explained in Section 5, the high value of average bond stress allowed by TR55 [13] leads

to overestimating the contribution of the DE FRP bars. Further experimental tests are recommended to confirm the FE predictions.

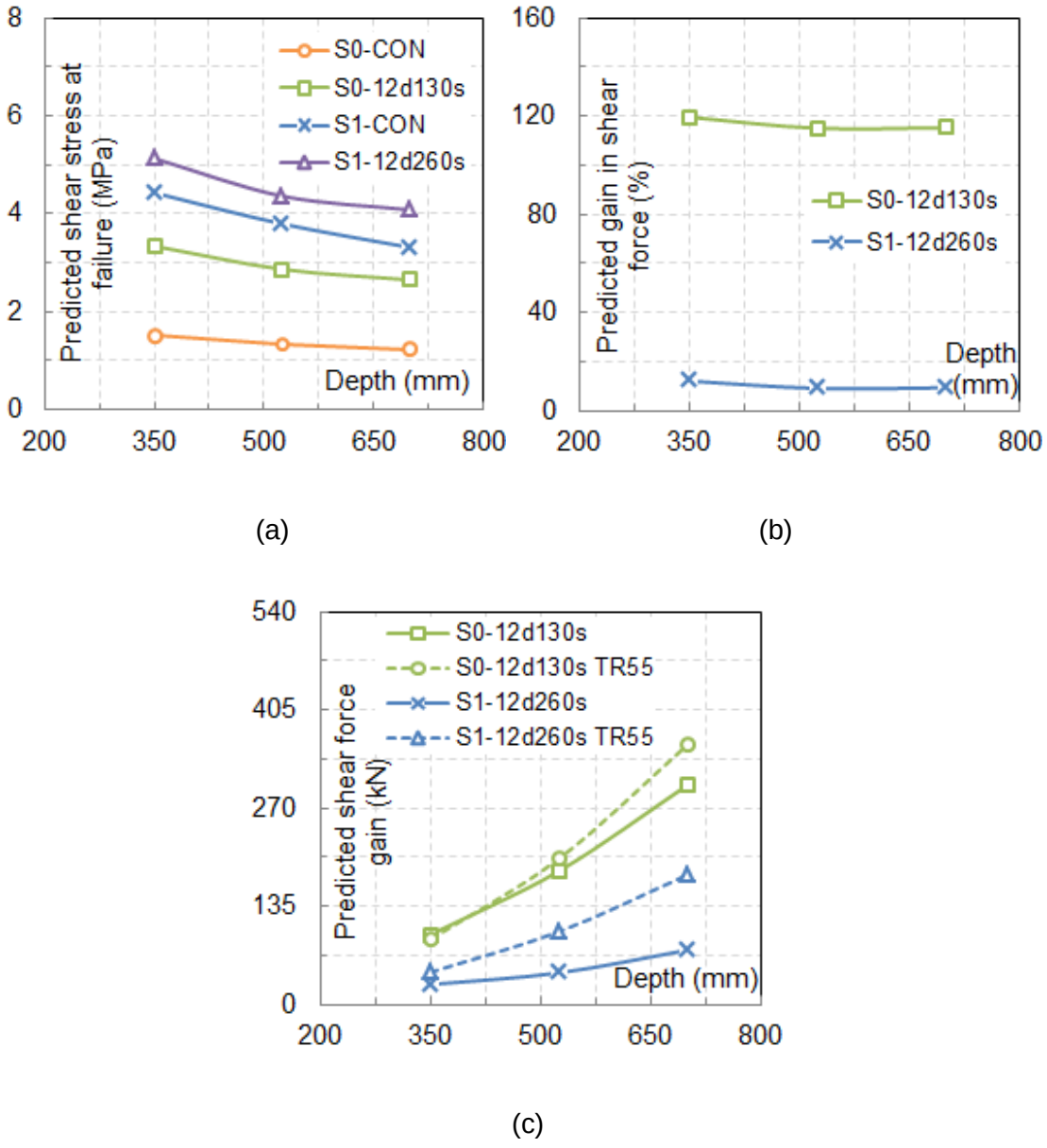

Fig. 15. Influence of effective beam depth on (a) the predicted shear stress at failure, (b) the percentage of shear force gain attributable to DE FRP bars and (c) the predicted shear force gain

6.5 Interaction between steel stirrups and DE FRP bars

For the case of RC beams shear-strengthened with EB FRP sheets [33,34], the presence of steel stirrups is one of the substantial parameters influencing the shear contribution of FRP

composites. The influence of the steel stirrup-to-DE FRP bar ratio was examined by modelling FE beams similar to S1-12d260s but with different steel stirrup-to-DE FRP bar ratios. The FE results are presented in Fig. 16 in terms of predicted shear force gain due to DE FRP bars versus $E_s.\rho_s/E_{frp}.\rho_{frp}$ (i.e. elastic modulus of steel stirrups multiplied by steel stirrups ratio / elastic modulus of DE FRP bars multiplied by DE FRP bars ratio). Based on the FE results, the predicted shear contribution of the DE FRP bars is inversely proportional to $E_s.\rho_s/E_{frp}.\rho_{frp}$.

Similar to the cases of DE FRP bar orientation, concrete compressive strength and a/d ratio, the TR55 design model [13] does not consider the interaction between steel stirrups and DE FRP bars. Consequently, the TR55 design model [13] might overestimate the shear strength enhancement for beams with high steel stirrup ratios. Further tests are required to confirm this result.

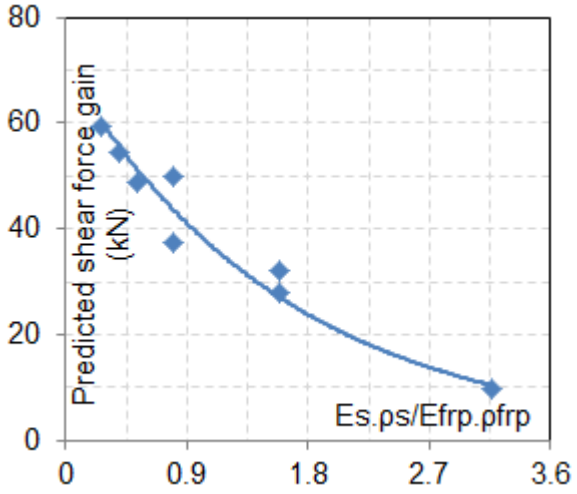

Fig. 16. Interaction between shear stirrups and DE FRP bars

7 Conclusions

A FE model for RC beams shear-strengthened with DE FRP bars was developed and validated using published experiments from the literature. The comparison of FE and TR55 predictions with experimental results demonstrates that the FE model is a significant

improvement over TR55 design model. The FE model had a mean predicted/experimental shear strength enhancement ratio of 1.08 (standard deviation of 0.25) whereas TR55 overestimated the shear strength enhancement with a mean predicted/experimental ratio of 1.57 (standard deviation of 0.54). A wide-ranging parametric study was conducted to study the influence of DE FRP bar orientation, concrete compressive strength, a/d ratio, effective beam depth and interaction between DE FRP bars and internal steel shear reinforcement on the predicted behaviour of RC beams strengthened in shear using DE FRP bars. The use of 45° inclined DE FRP bars, compared with vertical DE FRP bars, enhanced the predicted shear force capacity for beams with and without steel stirrups. The predicted shear strength enhancement was positively influenced by the increase in concrete compressive strength but decreased with increasing the a/d ratio and steel stirrup-to-DE FRP bar ratio. The increase in effective beam depth did not have a substantial influence on the percentage shear strength enhancement offered by the DE FRP bars. Compared to the FE results, TR55 design model overestimated the influence of effective beam depth on the shear strength enhancement, especially for the case of strengthened beams with shear links. TR55 does not consider the effect of DE FRP bar orientation, concrete compressive strength, a/d ratio and interaction between steel stirrups and DE FRP bars. Finally, it is noteworthy that the presented FE predictions reflect the performance of the developed model. Further experimental tests are therefore needed to confirm the FE predictions.

8 Acknowledgements

The financial support of the Engineering and Physical Sciences Research Council (EPSRC) through Grant EP/L010364/1 is gratefully acknowledged. The first author acknowledges the financial support of KRG. Additional data related to this publication is available at http://rab.bham.ac.uk/pubs.asp?id=6a980414-5a03-490a-b7b4-4fab77dd3cf5 or may be accessed via http://findit.bham.ac.uk.

9 References

1. ACI Committee 440. ACI 440.2R-08: Guide for the design and construction of externally bonded FRP systems for strengthening concrete structures. USA: Farmington Hills, 2008.
2. Belarbi A, Acun B. FRP systems in shear strengthening of reinforced concrete structures. Procedia Engineering 2013;57:2-8.
3. You Y, Ayoub A, Belarbi A. Three-dimensional nonlinear finite-element analysis of prestressed concrete beams strengthened in shear with FRP composites. ASCE Journal of Composites for Construction 2011;15(6):896-907.
4. Chaallal O, Mofidi A, Benmokrane B, Neale K. Embedded through-section FRP rod method for shear strengthening of RC beams: Performance and comparison with existing techniques. ASCE Journal of Composites for Construction 2011;15(3):374-383.
5. Motavalli M, Czaderski C, Pfyl-Lang K. Prestressed CFRP for strengthening of reinforced concrete structures: Recent developments at Empa, Switzerland. ASCE Journal of Composites for Construction 2011;15(2):194-205.
6. Dirar S, Lees JM, Morley CT. Precracked reinforced concrete T-beams repaired in shear with prestressed carbon fiber-reinforced polymer straps. ACI Structural Journal 2013;110(5):855-866.
7. Peng H, Zhang J, Cai CS, Liu Y. An experimental study on reinforced concrete beams strengthened with prestressed near surface mounted CFRP strips. Engineering Structures 2014;79:222-233.
8. Valerio P, Ibell TJ. Shear strengthening of existing concrete bridges. Structures and Buildings 2003;156(1):75-84.
9. Mofidi A, Chaallal O, Benmokrane B, Neale K. Experimental tests and design model for RC beams strengthened in shear using the embedded through-section FRP method. ASCE Journal of Composites for Construction 2012;16(5):540-550.

10. Barros J, Dalfré G. Assessment of the effectiveness of the embedded through-section technique for the shear strengthening of reinforced concrete beams. Strain 2013;49(1):75-93.
11. Qin S, Dirar S, Yang J, Chan A, Elshafie M. CFRP shear strengthening of reinforced-concrete T-beams with corroded shear links. ASCE Journal of Composites for Construction 2014;19(5):04014081.
12. Valerio P, Ibell TJ, Darby AP. Deep embedment of FRP for concrete shear strengthening. Structures and Buildings 2009;162(5):311-321.
13. The Concrete Society. Technical report TR55: Design guidance for strengthening concrete structures using fibre composite materials. Camberley: The Concrete Society, 2012.
14. Holicky M, Markova J, Sykora M. Assessment of deteriorating reinforced concrete road bridges. In: Bris R, Soares CG, Martorell S, editors. Reliability, risk and safety: Theory and applications. London: Taylor and Francis, 2010. p. 1377-1383.
15. ASCE Advisory Council. Report card for America's infrastructure. Reston, VA: ASCE, 2013. http://dx.doi.org/10.1061/9780784478837.
16. TNO DIANA BV. DIANA user's manual (release 9.4.4). Delft: TNO DIANA BV, 2012.
17. Bažant ZP, Oh BH. Crack band theory for fracture of concrete. Matériaux et Construction 1983;16(3):155-177.
18. Dirar S, Lees J, Morley C. Phased nonlinear finite-element analysis of precracked RC T-beams repaired in shear with CFRP sheets. ASCE Journal of Composites for Construction 2013;17(4):476-487.
19. Qapo M, Dirar S, Yang J, Elshafie MZEB. Nonlinear finite element modelling and parametric study of CFRP shear-strengthened prestressed concrete girders. Construction and Building Materials 2015;76:245-255.
20. Thorenfeldt E, Tomaszewicz A, Jensen JJ. Mechanical properties of high-strength concrete and applications in design. In: Proceedings of the Symposium on the Utilization of High-Strength Concrete, Stavanger, 15-18 June 1987. p. 149-159.

21. Vecchio FJ, Collins MP. Compression response of cracked reinforced concrete. ASCE Journal of Structural Engineering 1993;119(12):3590-3610.
22. Remmel G. Report No. 444: Zum zug-und schubtragverhalten von bauteilen aus hochfestem beton. Berlin: Deutscher Ausschuss für Stahlbeton, 1994. (In German)
23. fib. CEB-FIP model code 1990. London: Thomas Telford Services Ltd, 1993.
24. Hee SC, Jefferson AD. A new model for simulating cracks in cementitious composites. Engineering and Computational Mechanics 2008;161(1):3-16.
25. Arduini M, Tommaso AD, Nanni A. Brittle failure in FRP plate and sheet bonded beams. ACI Structural Journal 1997;94(4):363-370.
26. Vecchio FJ, Bucci F. Analysis of repaired reinforced concrete structures. ASCE Journal of Structural Engineering 1999;125(6):644-652.
27. Kani MW, Huggins MW, Kani G, Wittkopp RR. Kani on shear in reinforced concrete. Toronto: University of Toronto, 1979.
28. Sayed A, Wang X, Wu Z. Modeling of shear capacity of RC beams strengthened with FRP sheets based on FE simulation. ASCE Journal of Composites for Construction 2013;17(5):687-701.
29. Bažant ZP, Cao Z. Size effect of shear failure in prestressed concrete beams. ACI Journal 1986;83(2):260-268.
30. Tan KH, Cheng GH, Cheong HK. Size effect in shear strength of large beams behaviour and finite element modelling. Magazine of Concrete Research 2005;57(8):497-509.
31. Bousselham A, Chaallal O. Experimental investigations on the influence of size on the performance of RC T-beams retrofitted in shear with CFRP fabrics. Engineering Structures 2013;56:1070-1079.
32. Dirar S, Lees J, Morley C. Precracked reinforced concrete T-beams repaired in shear with bonded carbon fiber-reinforced polymer sheets. ACI Structural Journal 2012;109(2):215-224.

33. Khalifa A, Nanni A. Rehabilitation of rectangular simply supported RC beams with shear deficiencies using CFRP composites. Construction and Building Materials 2002;16(3):135-146.
34. Ary MI, Kang THK. Shear-strengthening of reinforced & prestressed concrete beams using FRP: Part I – Review of previous research. International Journal of Concrete Structures and Materials 2012;6(1):41-47.